

POSITION PAPER

2.65 Gbps Downlink Communications with Polarization Multiplexing in X-Band for Small Earth Observation Satellite

Tomoki KANEKO^{†a)}, Noriyuki KAWANO^{††}, Yuhei NAGAO^{†††}, *Nonmembers*, Keishi MURAKAMI^{††††},
 Hiromi WATANABE^{†††††}, Makoto MITA^{††}, *Members*, Takahisa TOMODA^{††††}, Keiichi HIRAKO^{†††††},
 Seiko SHIRASAKA^{†††††}, Shinichi NAKASUKA^{††††††}, *Nonmembers*, Hirobumi SAITO^{††}, *Member*,
 and Akira HIROSE[†], *Fellow*

SUMMARY This paper reports our new communication components and downlink tests for realizing 2.65 Gbps by utilizing two circular polarizations. We have developed an on-board X-band transmitter, an on-board dual circularly polarized-wave antenna, and a ground station. In the on-board transmitter, we optimized the bias conditions of GaN High Power Amplifier (HPA) to linearize AM-AM performance. We have also designed and fabricated a dual circularly polarized-wave antenna for low-crossstalk polarization multiplexing. The antenna is composed of a corrugated horn antenna and a septum-type polarizer. The antenna achieves Cross Polarization Discrimination (XPD) of 37 – 43 dB in the target X-band. We also modify an existing 10 m ground station antenna by replacing its primary radiator and adding a polarizer. We put the polarizer and Low Noise Amplifiers (LNAs) in a cryogenic chamber to reduce thermal noise. Total system noise temperature of the antenna is 58 K (maximum) for 18 K physical temperature when the angle of elevation is 90° on a fine winter day. The dual circularly polarized-wave ground station antenna has 39.0 dB/K of Gain - system-noise Temperature ratio (G/T) and an XPD higher than 37 dB. The downlinked signals are stored in a data recorder at the antenna site. Afterwards, we decoded the signals by using our non-real-time software demodulator. Our system has high frequency efficiency with a roll-off factor $\alpha = 0.05$ and polarization multiplexing of 64APSK. The communication bits per hertz corresponds to 8.41 bit/Hz (2.65 Gbit/315 MHz). The system is demonstrated in orbit on board the RAPid Innovative payload demonstration Satellite (RAPIS-1). RAPIS-1 was launched from Uchinoura Space Center on January 19th, 2019. We decoded 10^{10} bits of downlinked R- and L-channel signals and found that the downlinked binary data was error free. Consequently, we have achieved 2.65 Gbps communication speed in the X-band for earth observation satellites at 300 Mega symbols per second (MSPS) and polarization multiplexing of 64APSK (coding rate: 4/5) for right- and left-hand circular polarizations.

key words: *satellite communications, small satellite, DVB-S2X, Cross Polarization Discrimination (XPD), polarization multiplexing*

Manuscript received October 7, 2019.

Manuscript revised March 6, 2020.

Manuscript publicized July 1, 2020.

[†]The authors are with the Department of Electrical Engineering and Information Systems, The University of Tokyo, Tokyo, 113-8656 Japan.

^{††}The authors are with Institute of Space and Astronautical Science, Japan Aerospace Exploration Agency, Sagami-hara-shi, 252-5210 Japan.

^{†††}The author is with Radrix Co. Ltd., Iizuka-shi, 820-8502 Japan.

^{††††}The authors are with Synspec Inc., Tokyo, 135-0022 Japan.

^{†††††}The authors are with Keio University, Yokohama-shi, 223-8521 Japan.

^{††††††}The author is with the Department of Aeronautics and Astronautics, The University of Tokyo, Tokyo, 113-8656 Japan.

a) E-mail: kaneko.tomoki@eis.t.u-tokyo.ac.jp

DOI: 10.1587/transcom.2019EBN0009

1. Introduction

Technologies of small satellites are developing rapidly, resulting in the realization of constellation missions of small satellites. In particular, Synthetic Aperture Radar (SAR) missions require big downlink capacity [1]. However, the communication speeds of conventional small satellites are not enough to realize such constellation missions. In this paper, we focus on the development of high speed downlink communications for small satellites.

Conventional medium and large earth observation satellites utilize the X-band for their observation-data downlink with 0.3–0.6 Gbps by using a single polarization. They commonly use Quadrature-Phase Shift Keying (QPSK) or 8-ary Phase Shift Keying (8PSK) to avoid the nonlinearity problems of High Power Amplifiers (HPAs). A large optical satellite, WorldView-3 achieved 1.2 Gbps downlink with polarization multiplexing, 8PSK modulation and 200 Mega symbol per second (MSPS) rate in the X-band [2].

Table 1 shows a comparison of the work in this paper with conventional satellite communication systems. A large SAR satellite, ALOS-2, accomplished 0.8 Gbps by using 16 Quadrature-Amplitude Modulation (16QAM) with 200 MSPS in the X-band [3]. In fact, their effective communication speeds considering the coding rate of an error correction code are smaller than the above-mentioned values. Their frequency efficiency is also low.

In 2019, cubesats of Planet Lab achieved 1.6 Gbps downlink with dual polarization channels in the X-band [5]. Each of the dual polarization channels is multiplexed in the frequency domain in three frequency bands with 32 Amplitude-Phase Shift Keying (APSK) of 76.8 MSPS. The XPD in their downlink system is about 20 dB, which is determined mainly by an on-board antenna.

Two issues have to be solved in order to increase the communication speed furthermore. One is the issue of guard band in frequency division multiplexing, which causes loss of frequency bandwidth. Another is the issue of low XPD in the downlink system, which degrades link budget especially for higher modulation scheme such as 64APSK.

In ground communications, Orthogonal Frequency Division Modulation (OFDM) is widely used to eliminate its guard band. In 2015, High Throughput Satellites (HTSs) have been studied. They often utilize frequency multiplex-

Table 1 Comparison of this work with conventional satellite communication systems.

paper	Frequency	Bandwidth	Multiplexing	Modulation	Type	Data rate	Frequency efficiency
[2]	X-band	375 MHz	Polarization	8PSK	Downlink / LEO*	1.2 Gbps	3.20 bit/Hz
[4]	X-band	375 MHz	None	16QAM	Downlink / LEO*	0.8 Gbps	2.13 bit/Hz
[5]	X-band	288 MHz	Polarization & frequency	32APSK	Downlink / LEO*	1.6 Gbps	5.56 bit/Hz
[6]	Ka-band	940 MHz	Frequency	16APSK & 16QAM	Bent-pipe / GEO**	3.2 Gbps	3.40 bit/Hz
This work	Xband	315 MHz	Polarization	64APSK	Downlink / LEO*	2.65 Gbps	8.41 bit/Hz

*LEO: Low-Earth orbit

**GEO: Geostationary-Earth orbit

ing with OFDM. The team of National Institute of Information and Communications Technology (NICT) achieved 3.2 Gbps in Ka-band in a geostationary orbit satellite by using 16APSK and 16QAM based on DVB-S2X [6]. This is a bent-pipe communication system between ground stations and a geostationary satellite, where there is no Doppler effect. They try to develop a HTS with polarization multiplexing for realizing further high speed communication [7].

However, OFDM is sensitive to frequency shift and is hardly applied to low earth orbit satellites with Doppler frequency shift. In order to increase the downlink speed for low-orbit earth observation satellites, it is reasonable to use a single carrier modulation. Recent signal processing technologies make it possible to develop a single carrier modulation system with 300 Msps.

This paper reports a high-data-rate and high-spectrum-efficiency downlink system using 64APSK, polarization multiplexing, and a small roll-off factor. Additionally, we have developed a ground station system with a high-XPB and high-G/T ground station antenna and a 300-Msps demodulator.

We realize the high bit rate downlink with the following three key points. First, we obtain high quality 64APSK signals by optimizing the operation point of a HPA, which realizes a small third-order distortion. Secondly, we used a high XPB antenna that we designed to minimize polarization interference [8]. Thirdly, we have developed a ground station system with a high-XPB and high-G/T ground station antenna.

The system has a high frequency efficiency with a roll-off factor $\alpha = 0.05$ and polarization multiplexing of 64APSK. Then, the communication bits per hertz corresponds to 8.41 bit/Hz (2.65 Gbit/315 MHz). The performance has been demonstrated in orbit on board of RAPIS-1 (RAPid Innovative payload demonstration Satellite 1) designed with one-year life time by Japan Aerospace Exploration Agency (JAXA) [9], [10]. In June 2019, we have achieved 2.65 Gbps downlink satellite communication with 300 Msps and polarization multiplexing of 64APSK (4/5) for Right-Hand Circular Polarization (RHCP) and Left-Hand Circular Polarization (LHCP), respectively, in the X-band.

This paper is organized as follows. Section 2 presents the communication system design. Section 3 describes an on-board X-band transmitter. Section 4 explains an on-board dual circularly polarized-wave antenna while Sect. 5 describes a ground station. Section 6 reports the downlink results. Section 7 is the conclusions.

2. Communication System Design

2.1 Total System Construction

In this section, we deal with our high data-rate downlink system shown in Fig. 1, including an on-board transmitter, an on-board dual circularly polarized-wave antenna, and a high G/T and XPB ground station antenna. Then, Tables 2, 3, and 4 list specifications of our new communication system.

2.2 DVB-S2X Standard

The DVB-S2X standard is an extension version of the DVB-S2, which has been mainly applied to geostationary broadcasting and communication satellites. It contains wide range of modulation schemes from QPSK to 256APSK and the minimum roll-off factor $\alpha = 0.05$ in the Square-Root-Raise-Cosine (SRRC) filter [11], [12]. Then, we select this standard for our high data-rate downlink system since it is suitable for communications having a high frequency efficiency.

DVB-S2X standard has a length of 64,800 bits in a normal frame, and an error correction code named Low Density Parity check Code (LDPC) [13]. LDPC needs a large amount of calculation cost due to the numerical iteration. Additionally, the standard is easy for the equalizer design because the pilot signals are located in several points in a frame.

2.3 Symbol Rate and Occupied Frequency

A frequency band of 8.025 – 8.4 GHz (375 MHz bandwidth) is allocated for a downlink of the earth observation data. There is a deep space downlink band at 8.4 – 8.45 GHz. International Telecommunication Union (ITU) recommends a criteria for a deep space band protection in ITU SA1157-1 [14]. The protection criteria for a deep space earth-station receiver at an input terminal (Low Noise Amplifier (LNA)) is less than -221 dB (W/Hz) in 8.4 – 8.45 GHz.

Our ground station antenna is located near Usuda Deep Space Center, JAXA, where there is a 64 m diameter antenna (72.5 dBi gain in the X-band) for deep space communications. Then, the ITU requirement is severe compared with an usual frequency band allocation. It is estimated that the 64 m antenna receives the in-band signal level of -165 dB (W/Hz). Then, we have to attain an out-of-band signal level (8.4 – 8.45 GHz) more than 56 dB (=

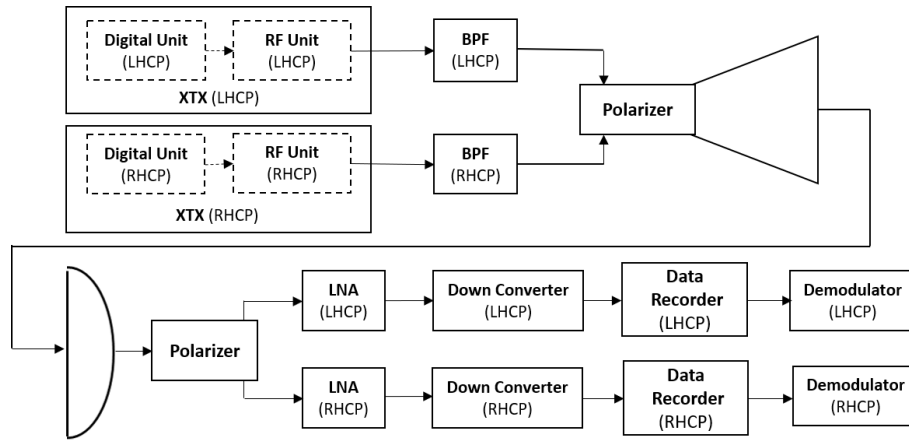


Fig. 1 System block diagram of a high speed downlink where the upper part is an on-board segment while the lower part is a ground segment.

Table 2 Specification of the communication system.

Frequency	8.025 – 8.34 GHz
Occupied Bandwidth	315 MHz
Symbol Rate	300 Msps
Modulation	QPSK – 64APSK (256APSK)
Bit Rate	Max 2.65 Gbps/2 ch
Roll-off Factor	0.05
Communication Standard	DVB-S2X
Error Correction Code	LDPC, BCH
Polarization Channel	RHCP/LHCP 2 ch
Total XPD*	> 27 dB

*The total XPD includes atmospheric effects.

Table 5 Communication data-rate for various modulations and coding rates.

Modulation	Coding Rate	Data-Rate (Gbps)*
QPSK	13/45	0.160
16APSK	26/45	0.479
64APSK	132/180	1.214
64APSK	4/5	1.325

*For example, the data rate of 64APSK (4/5) is calculated as
 Data Rate = (symbol rate) × (bits per symbol) × (coding rate)
 × (1 – ratio of frame gap) × (ratio of data without known signal)
 = 300×10⁶ × 6 × 4/5 × (1 – 0.05) × (10800/(10800+36×7+90))
 See also Fig. 9.

Table 3 Specification of the on-board transmitter and antenna.

Transmitter	RF Power	29.5 dBm/ch
	DC Power	75 W/2ch
	Size	20 cm × 20 cm × 20 cm
	Weight	6 kg
	Antenna	Type
Gain		17 dBi
XPD		> 37 dB

Table 4 Specification of the ground station antenna.

Antenna	10m Cassegrain
Ant Gain	56.6 dBi at Pol input
Ant XPD	> 37 dB
LNA noise temperature	5 K in a cryogenic chamber
System noise temperature	58 K at EL 90°
Ant G/T	39 dB/K at EL 90°

Table 6 Link calculation of our downlink with 64APSK (4/5).

Orbit Altitude	510.0	km
Elevation	20.0	deg
Center Frequency	8.2	GHz
Symbol Rate	300.0	Msps
RF power	29.5	dBm
Tx Cable Loss	1.5	dB
Tx Ant Gain	17.0	dBi
Prop. Loss	172.4	dB
Rx Ant Gain	56.6	dBi
System noise temperature	58.0	K
Received C/N	110.4	dB
Received E _s /N ₀	25.6	dB
Req E _s /N ₀	19.5	dB
Margin	6.1	dB

the group delay of the BPF for a deep-space band protection.

2.4 Link Calculation

We calculated the link budget of our downlink system. Table 5 lists the communication data-rates for various modulation schemes. Table 6 lists a result of link calculation.

The document of DVB-S2X standard describes the required E_s/N₀ (E_s: signal energy per symbol, N₀: noise energy) for 10⁻⁵ of Frame Error Rate (FER) with the Non-Linear Hard Limiter Channel at a Traveling Wave Tube Amplifier (TWTA) [15]. Here, the required E_s/N₀ is given as 19.5 dB for 64APSK with 4/5 of coding rate. Under this

–165 dB (W/Hz) – (–221 dB (W/Hz)) compared to the in-band level (8.025 – 8.34 GHz).

Transmitters radiate out-of-band with a certain level. The level is mainly dependent on the third-order distortion in a HPA. We trimmed the bias conditions and the input power level so that the third-order distortion is as low as –30 dB. Additionally, we have to insert a Band-Pass Filter (BPF) which has an attenuation level of higher than 26 dB (= 56 – 30 dB) at 8.4 – 8.45 GHz. We determined the bandwidth of 8.025–8.34 GHz with 315 MHz/(1+α) = 300 Msps based on

Table 7 Parameters in the rainfall region K in [18].

R (mm/h)	p (%)	σ (°)
1.5	1.00	0.0
4.2	0.30	2.7
12.0	0.10	5.0
23.0	0.03	7.6

assumption, the link with 64APSK (4/5) has 6.1 dB margin at 20° of elevation shown in Table 6.

2.5 Dual Polarization Channels

It is effective to utilize the dual circularly polarized wave to double the communication speed. However, the crosstalk between the two polarization channels degrades the communication quality. Then, we have developed communication antennas with a crosstalk as low as possible because the crosstalk between RHCP and LHCP is not cancelled in the present system. The Cross Polarization Discrimination (XPD), which is defined as the power ratio of the main polarization signal to the cross one, is an index to evaluate the crosstalk effect.

It is reported that an atmospheric XPD on a fine day is 30 – 35 dB in the X-band [16]. The XPD is degraded by the effect of ice in cloud and rain. A rainy-day XPD is modeled as [17]

$$XPD_{\text{rain}} = C_f + C_A + C_\tau + C_\theta + C_\sigma \quad (1)$$

$$\begin{cases} C_f = 60 \log f - 28.3 \\ C_A = 30.8 f^{-0.21} \log A_p \\ C_\tau = -10 \log(1 - 0.484(1 + \cos 4\tau)) \\ C_\theta = -40 \log(\cos \theta) \\ C_\sigma = 0.0053 \sigma^2 \end{cases} \quad (2)$$

where f (GHz) and θ (°) are frequency and the angle of elevation, A_p (dB) and τ (°) are rain attenuation and tilt angle, and σ (°) is the effective standard deviation of the raindrop scattering angle distribution. There, τ is 45° for circularly polarized wave, σ takes the value 0°, 5°, 10°, and 15° for 1%, 0.1%, 0.01%, and 0.001% of the time percentage, respectively, and f takes the value of 8.2. We estimate σ with a percentage of time p (%) for various rainfall rate as shown in Table 7 [17], [18].

A rain attenuation A_p is defined as [17], [19]

$$A_p = \gamma_R D_{\text{rain}} \quad (3)$$

$$\begin{cases} \gamma_R = K R^\alpha \\ D_{\text{rain}} = \frac{h_{\text{RAIN}} - h_{\text{ANTENNA}}}{\sin \theta} \\ h_{\text{RAIN}} = 5 - 0.0075(\Phi - 23) \end{cases} \quad (4)$$

where Φ ($= 36.13^\circ$), h_{ANTENNA} ($= 1.5$ km), and R are latitude, altitude of the antenna, and rainfall rate respectively. Then, K and α with a circularly polarized wave at 8 GHz are approximated as an average value of the horizontally and vertically polarized waves, and are calculated as 0.00425 and 1.3185, respectively [20]. An atmospheric XPD including

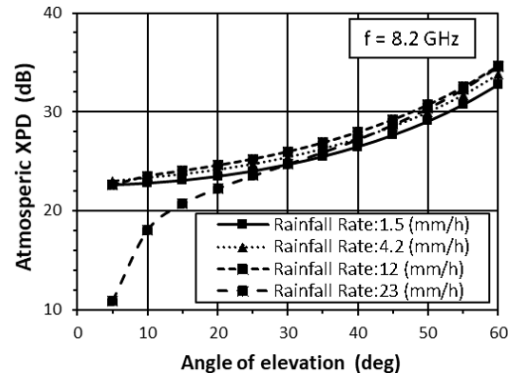


Fig. 2 An atmospheric XPD verses angle of elevation for various rainfall rate at 8.2 GHz.

the effects of ice in cloud and rain is given by [17]

$$\begin{cases} XPD_A = XPD_{\text{rain}} - C_{\text{ice}} \\ C_{\text{ice}} = XPD_{\text{rain}} \frac{0.3 + 0.1 \log p}{2} \end{cases} \quad (5)$$

where XPD_A (dB) is an atmospheric XPD. Figure 2 shows XPD_A verses angle of elevation for various rainfall rate at 8.2 GHz. We have estimated the XPD_A as 28 dB in 45° of elevation with 4.2 (mm/h) rainfall rate at 8.2 GHz.

The total XPD of the communication system is expressed as [15]

$$XPD_{\text{total}} = (XPD_{\text{Tx}}^{-1} + XPD_{\text{Rx}}^{-1} + XPD_A^{-1})^{-1} \quad (6)$$

where XPD_{Tx} and XPD_{Rx} are XPDs of the transmitting and receiving antennas, respectively.

In addition to the degradation of XPD with atmospheric propagation, an XPD is degraded by the transmitting and receiving antennas. In this system, we need an XPD of the antennas least four times as high as the XPD_A ($XPD > 34$ dB). Then, we have developed the on-board and ground-station antennas with an XPD of the antennas higher than 37 dB. The XPD of the total communication system is calculated in (6) as 27 dB.

3. X-band Transmitter

3.1 Evaluation System of X-Band Transmitter

Figure 3 shows an evaluation system of X-band transmitter (XTX) in a laboratory room. In a development stage of the XTX, we evaluated the XTX consisting of the Keysight evaluation system consisting of an oscilloscope, 89600VSA software, and System Vue. The output signals in the transmitter are sent to the BPF for the deep space protection. Afterwards, the X-band signals are down-converted to Intermediate Frequency (IF) signals and digitized by the oscilloscope. The signals are decoded by Keysight System Vue DVB-S2X library [21]. An evaluation index of the XTX is Error Vector Magnitude (EVM) after an equalizer in System Vue [22].

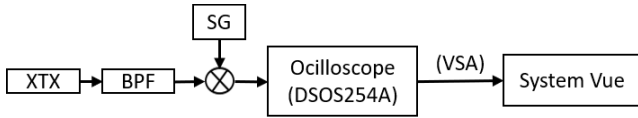


Fig. 3 An evaluation system of X-band transmitter in a laboratory room.

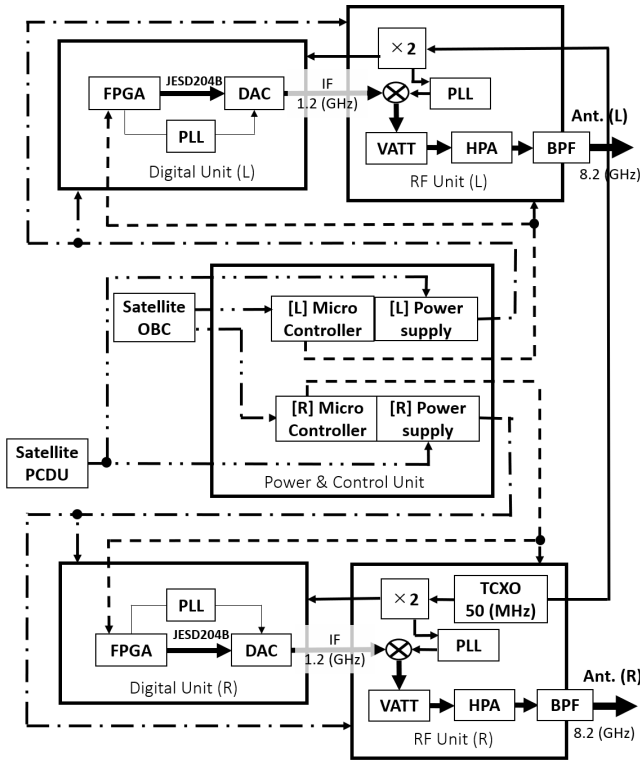
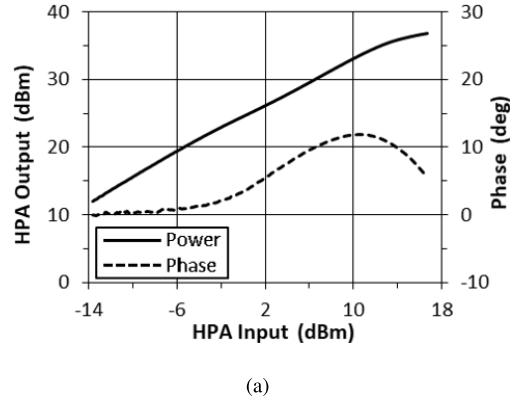


Fig. 4 Block diagram of the Digital Unit, the RF Unit and the Power&Control Unit in the XTX.

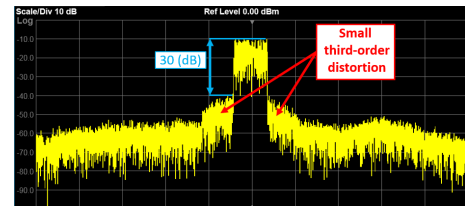
3.2 Structure of XTX

Figure 4 shows a block diagram of the XTX. The XTX is composed of the two transmitters for RHCP and LHCP. Each channel is composed of the Digital Unit, the RF Unit, and the common Power & Control Unit. These units are assembled with high rigidity titanium rods and washers.

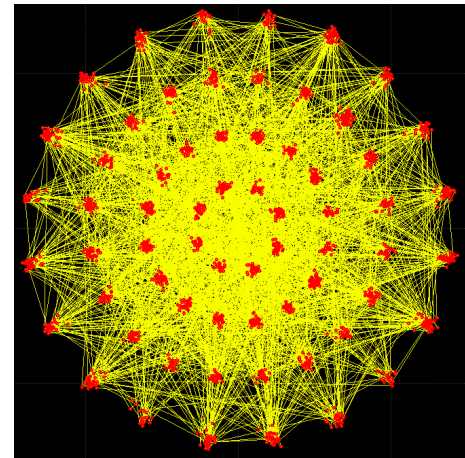
The Digital Unit has a FPGA with a Ball Grid Array (BGA) instrumentation. The In-phase and Quadrature-phase (IQ) signals produced in the FPGA are processed with a SRRRC filter. The digital IQ signals are sent to an external DAC with JESD204B, which is a several Gbps class high speed communication protocol [23]. Then, the IF modulated signals of 1.2 GHz are generated at the DAC. The analogue IQ signals are sent to the RF Unit. A Phase Locked Loop (PLL) generates a local frequency of 7 GHz with a crystal oscillator. The IF modulated signals are up-converted to the X-band by the 7 GHz. Afterwards, the X-band signals are amplified by driver amplifiers and a GaN High Electron Mobility Transistor (HEMT) two-stage HPA. The amplified signals become its 29.5 dBm of its RF power. Then, the



(a)



(b)



(c)

Fig. 5 (a) An AM-AM and AM-PM characteristics in a HPA, (b) a spectrum at a HPA, and (c) a constellation of 64APSK (4/5) at the XTX output [9].

signals are sent to the BPF for the deep space band protection. The semiconductor devices have 10 krad radiation resistance, corresponding to 5 years.

3.3 Third-Order Distortion at HPA in XTX

The EVM is one of the performance indices of a transmitter. It quantitatively represents the difference between observed and ideal signals in a plane of In-phase and Quadrature-phase components. A large difference leads to the degradation of communication quality, resulting in a higher bit error [24]. The bias conditions and the output power level in a HPA are important to obtain a high quality signal. We evaluate the

third-order distortion based on an AM-AM characteristics in a HPA [25].

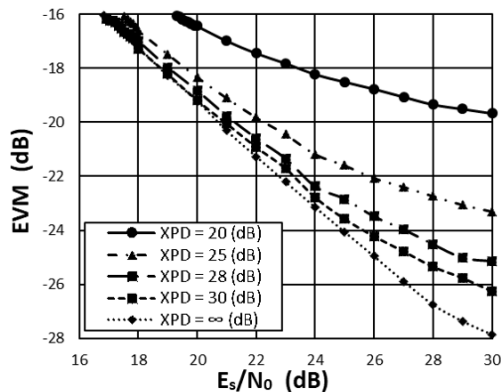
Figure 5 shows (a) an AM-AM/AM-PM characteristics, (b) a spectrum at a HPA (before the BPF), and (c) a constellation of 64APSK (4/5) at the XTX output [9], [10]. We trimmed the input power and the bias conditions with the average output power fixed at 29.5 dBm. Then, the AM-AM curve becomes almost linear and the AM-PM curve keeps monotonic increase up to around the average power as shown in Fig. 5(a). Figure 5(b) indicates that the third-order distortion is suppressed as low as -30 dB compared with the in-band level. A constellation of 64APSK (4/5) is shown in Fig. 5(c). The measured EVM of R-channel is -28.5 dB while that of L-channel is -29.8 dB.

3.4 Degradation of Signal Quality Due to Crosstalk

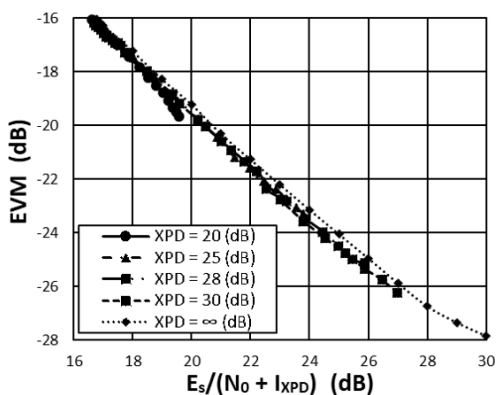
It is effective to transmit two independent information by multiplexing RHCP and LHCP. However, we need the high XPD transmitting and receiving antennas because the crosstalk between the two polarization channels degrades the communication quality in the unsynchronized Pseudo Ran-

dom Binary Sequence (PRBS) downlink system [26], [27].

We evaluated the quality degradation of the 1.2 GHz IF signal at the Digital Unit output due to the crosstalk. We output the dual channel signals recorded in a data storage. Then, we combined the main channel signal with the crosstalk attenuated to a certain level to produce a signal including a crosstalk. After we digitalized the signal by an oscilloscope, we added thermal noise to the signal with System Vue. Then, we analyzed the signal including the crosstalk and the thermal noise for 5,128,288 bits (= 100 frames) by using System Vue until bit error occurs. Figure 6(a) shows the measured EVM for the IF signal at the Digital Unit output versus the thermal noise for various XPD. The Bit Error Rate (BER) is less than 10^{-6} when $\text{EVM} \leq -16.1$ dB. Figure 6(a) indicates that, for example, when E_s/N_0 is 25 dB with an XPD of 25 dB, the EVM is larger by 2 dB than that when $\text{XPD} = \infty$. The floor shown in Fig. 6(a) is attributed to the phase noise of Temperature-compensated crystal Oscillator (TCXO) and the reflection at the Digital Unit output connector after the DAC. Figure 6(b) represents that the EVM against $E_s/(N_0 + I_{\text{XPD}})$ is plotted in a line with about less than 0.5 dB deviation at 20, 25, 28, 30 ∞ dB of XPD where I_{XPD} is a crosstalk interference. Figure 6(b) also means that the crosstalk can be dealt with approximately as thermal noise.



(a)



(b)

Fig. 6 (a) EVM versus E_s/N_0 and (b) EVM versus $E_s/(N_0 + I_{\text{XPD}})$ for various XPD when we add thermal noise to the IF signal including the crosstalk in System Vue.

4. Dual Circularly Polarized-Wave Antenna

We utilize the two channels of RHCP and LHCP in order to double the communication speed. We have developed a dual circularly polarized-wave antenna composed of a corrugated horn antenna and a septum-type polarizer. The antenna has an aperture diameter of 140 mm and a length of 104 mm. It is well known that a circular corrugated horn structure is suitable for a wide band high XPD medium gain antenna [28]. The XPD of the on-board system is thus mainly determined by the polarizer which produces right and/or left circularly polarized wave [29].

Using an ANSYS/HFSS electromagnetic simulator, we designed and fabricated a septum-type polarizer and a corrugated horn antenna. Figure 7 shows pictures of (a) the dual circularly polarized-wave antenna (on-board antenna) [9] and (b) the septum-type polarizer [27]. The measured gain of the on-board antenna is 17 dBi.



(a)

(b)

Fig. 7 Pictures of (a) the dual circularly polarized-wave antenna [9] and (b) the septum-type polarizer [27].

Figure 8 shows the measured and design XPD values versus of XPD versus frequency [27]. We measured the axial ratio of the on-board antenna to evaluate its XPD. Then, we fixed the on-board antenna, while we rotated the aperture of a transmitting pyramidal horn antenna around the boresight axis by 360° with 1° step. Afterwards, we obtained the axial ratio with the difference between maximum and minimum received power. The value of the axial ratio is converted to the value of XPD. Figure 8 indicates 37 – 43 dB of XPD in 8.025 – 8.34 GHz.

5. Ground Station

5.1 High XPD and G/T Ground Station Antenna

Our downlink system requires a high XPD performance for the low-crosstalk polarization multiplexing. Most conventional ground station antennas have 20 – 25 dB of XPD, which is not enough for our new downlink system [5]. We have modified an existing 10 m antenna in Usuda Space Center. The antenna was constructed in the 1980s for a Ku-band downlink of a space VLBI satellite “HARUKA.” We have renewed its primary radiator.

Candidates of the primary radiator are a corrugated horn antenna and a dual-mode horn antenna. However, a fabri-

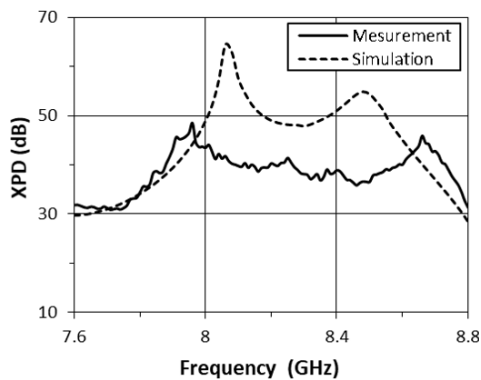


Fig. 8 XPD versus frequency with the dual circularly polarized-wave antenna [27].

cation of a large corrugated horn antenna is very difficult. Then, we selected a dual-mode horn antenna. The ground station antenna has a designed gain 56.6 dBi and an aperture efficiency of 67% at the input port of the primary feeder in the X-band.

The primary feeder horn antenna in the Cassegrain antenna is connected to the polarizer through a 1.5 m circular waveguide. The septum-type polarizer and the coaxial LNAs are cooled down to 18 K physical temperature in a cryogenic chamber. When the angle of elevation is 90° on a fine winter day at 15 K of sky temperature, a measured system noise temperature in the ground station antenna is 52 – 58 K in the 8.0 – 8.4 GHz by using the Y-factor method. Thus, Gain - system-noise Temperature ratio (G/T) is calculated as 39 dB/K.

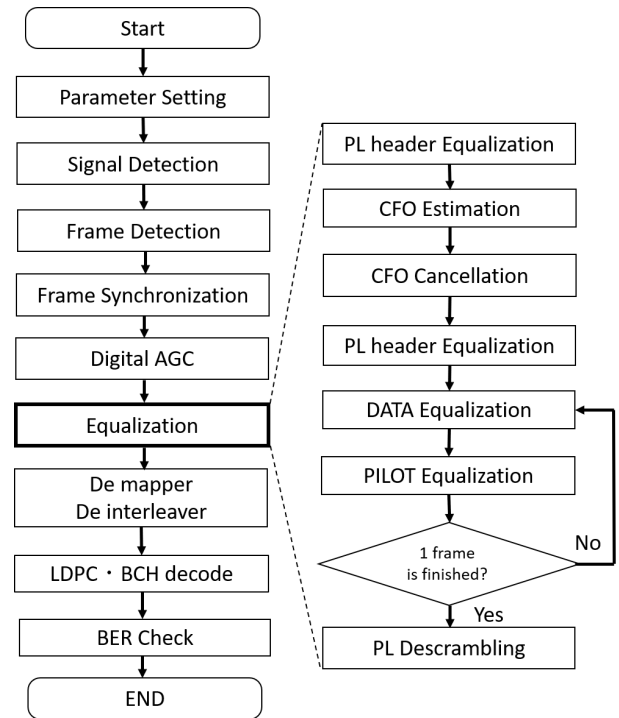


Fig. 10 The sequence of demodulation process.

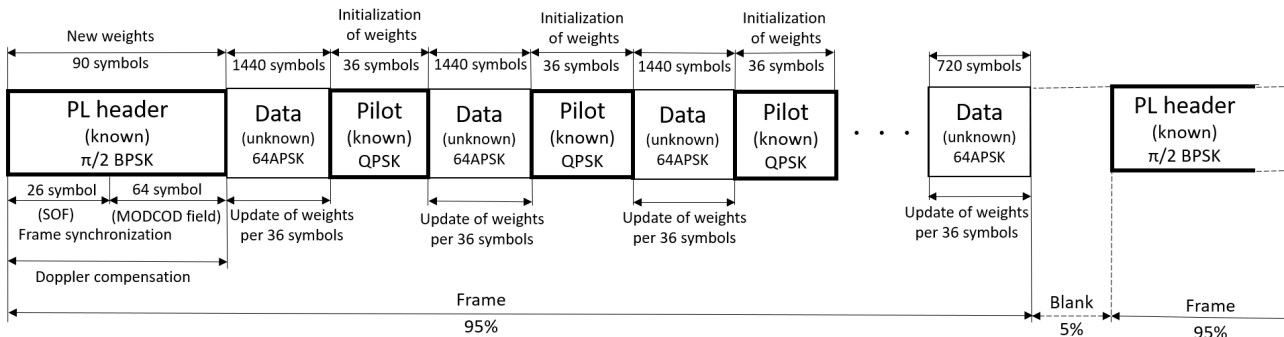


Fig. 9 A format of DVB-S2X frame with the pilot signals. The 64APSK data in the frame has 10800 symbols. After 1440 symbols of data, the 36 symbols of the pilot signals are inserted. The combinations of them are allocated 7 times in the frame. The last group of data has 720 symbols (= 10800 – 1440 × 7) In addition, this figure explains the equalization process.

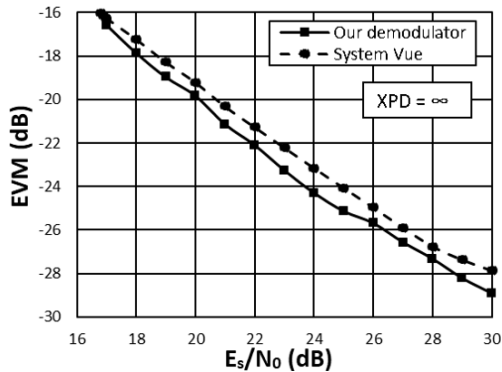
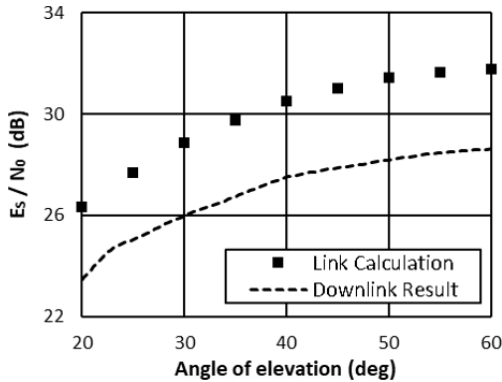
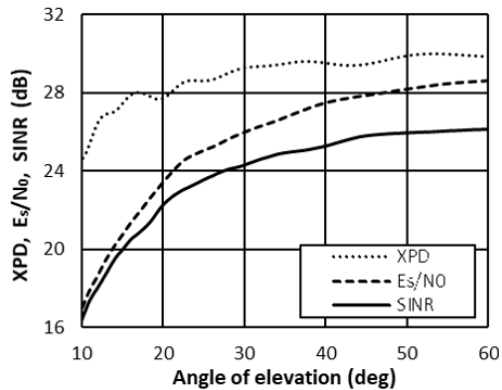


Fig. 11 A comparison of our demodulator with the System Vue (reference demodulator). We analyze signal quality with 64APSK (4/5). We add thermal noise to the signal without the crosstalk and the Doppler effects for $BER \leq 10^{-6}$ in a laboratory room experiment.



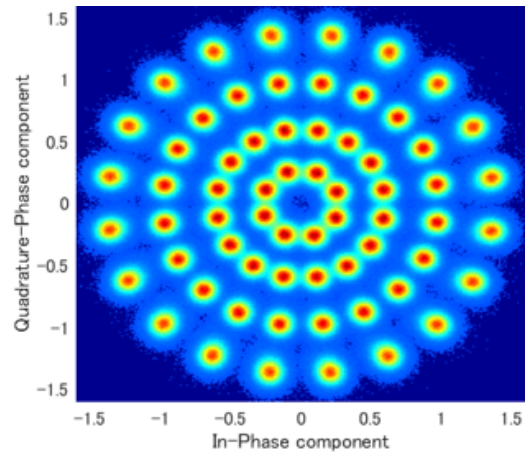
(a)



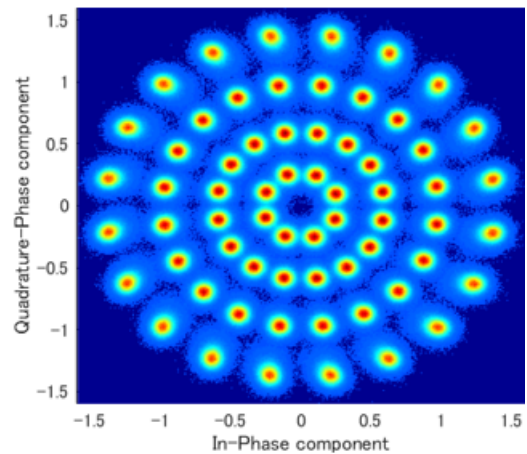
(b)

Fig. 12 (a) E_s/N_0 versus angle of elevation in calculation and experiment, and (b) XPD, E_s/N_0 , and channel SINR ($E_s/(N_0 + I_{XPD})$) versus angle of elevation with 510 km of the satellite altitude in L-channel experiment.

The designed value of XPD due to a surface accuracy of the main dish is about 52 dB. A measured value of the XPD at the primary radiator is 45 dB. The septum-type polarizer in the ground station is identically designed as one for the on-board antenna. The XPD of polarizer was measured to



(a)



(b)

Fig. 13 64APSK (4/5) constellation of downlinked (a) R- and (b) L-channel signals.

be higher than 37 dB at 18 K physical temperature. Thus, the total XPD of the ground station antenna is estimated as higher than 37 dB.

5.2 Our 300-Msps Demodulator

Our purpose is to demonstrate the high downlink speed. No DVB-S2X standard hardware demodulator with 300 Msps is available at present. Then, we have developed the non-real-time software demodulator combined with a data storage system. The received dual signals are down-converted to 1.4 GHz at the antenna site, and are AD-converted into digital baseband signals to be stored by a data recorder.

Figure 9 shows a format of 64APSK DVB-S2X frame with the pilot signals. Figure 10 shows the sequence of the demodulation process. There are 5% no-signal periods between frames. The demodulator finds a header of the frame based on the average power level of the received signal. The received signal is synchronized with a matched filter by us-

Table 8 Downlink experiment conditions: acquisition Of Signal (AOS), state of weather, modulation scheme, SINR, elevation of antenna and resulting XPD.

AOS (UTC)	Temp (°C)	Cloud cover (%)	Rainfall rate (mm/h)	Modulation scheme	SINR (dB)	EL (°)	XPD (dB)
May. 20, 2019, 00:32:03	17.8	0	0	64APSK (132/180)	23.2	45	27.0
May. 21, 2019, 00:15:03	15.9	100	6.5	64APSK (132/180)	23.3	45	28.6
Jun. 23, 2019, 00:29:07	15.0	50	0	64APSK (4/5)	25.3	45	29.2
Jun. 24, 2019, 00:12:38	10.8	100	0.7	64APSK (4/5)	24.4	45	28.6
Feb. 14, 2020, 00:28:40	3.7	100	0	QPSK (13/45)	21.4	30	30.7
Feb. 15, 2020, 00:21:46	1.7	100	0	QPSK (13/45)	25.7	30	31.7
Feb. 16, 2020, 00:15:03	5.7	100	1	64APSK (4/5)	25.1	30	31.6

Table 9 Stability of communication link after zenith showing various SINR on June 23, 2019.

Start time (UTC)	SINR (dB)	Elevation (°)	Number of Frames (time (s))	EVM(dB)	Mean number of LDPC iteration (-)	Frame error rate (-)
00:34:21	26	52.0	200000 (= 7.64)	-20.1	4.0	0
00:34:57	25	36.1	200000 (= 7.64)	-20.2	3.7	0
00:35:07	24	27.4	200000 (= 7.64)	-19.8	4.3	0
00:35:49	23	22.2	200000 (= 7.64)	-19.5	4.5	0
00:36:04	22	19.4	200000 (= 7.64)	-19.8	4.4	0
00:36:16	21	17.5	90000 (= 3.43)	-18.7	6.7	3.3×10^{-6}
00:36:33	20	15.0	60000 (= 2.29)	-18.1	6.5	1.0×10^{-5}
00:36:46	19	13.3	10000 (= 0.38)	-18.2	10.3	4.0×10^{-5}
00:36:58	18	11.8	10000 (= 0.38)	-17.9	16.7	3.7×10^{-4}

ing the 26 symbols of a Start Of Frame (SOF) preamble in the Physical Layer header (PL header). Afterwards, the amplitude of the synchronized signal is adjusted by an Automatic Gain-Controller (AGC). At the obtainment process of PL header, the signal is equalized as follows.

The channel impulse response is expressed as a product of an inverse Toeplitz matrix of the 90 symbol preamble in the PL header and the received signal. The optimal weights based on the least squares estimation are derived as the inverse Toeplitz matrix of the channel impulse response. Afterwards, we obtain the PL header from the product of Toeplitz received signal matrix and the weights [30]. We compensate the Carrier Frequency Offset (CFO) caused by the Doppler effect by using an averaged phase rotation in an open-loop manner. We use known-64 symbols at the MODCOD field in the PL header. After cancelling CFO, we equalize the PL header again.

The weights derived by the least squares estimation are updated per 36 symbols of the IQ data with the LMS algorithm [31]. However, under a low E_s/N_0 communication environment, inappropriate weights cause the phase rotation of the IQ data due to the insufficient Doppler compensation. To compensate the phase rotation, we set least-squares-estimation weights with the 36 symbols of the pilot signals. In addition, when the LDPC does not converge in iteration of fifty times, we execute a Bose-Chaudhuri-Hocquenghem (BCH) code in DVB-S2X standard.

When we evaluate our 300-Msps demodulator, we use System Vue as a reference demodulator. Figure 11 shows a comparison with the performance of System Vue and the demodulator. Then, we evaluate the performance of the demodulator decoding the signal by gradually increasing the level of thermal noise addition, without the crosstalk and the Doppler effects, for 5,128,288 bits (= 100 frames) in a

laboratory room until bit error occurs. Figure 11 shows that the demodulator can decode the signal down to 17.0 dB of E_s/N_0 without bit error while System Vue can decode one by 16.8 dB of E_s/N_0 at the top-left points. In short, the robustness in E_s/N_0 with the demodulator is 0.2 dB inferior to that of System Vue. In larger the E_s/N_0 region, our demodulator shows $EVM \approx -E_s/N_0$ approximately. The 1 dB degradation in System Vue is originating from the lack of compensation for the insufficient PLL center-frequency locking.

6. Downlink Results

In this section, we describe the downlink results. Our communication system has been demonstrated in orbit on board of RAPIS-1, JAXA. The RAPIS-1 was launched into 510 km altitude orbit from Uchinoura on January 19th, 2019.

The XTX outputs the R-channel signal 0.15 seconds later than the L-channel one. Then, we evaluate the XPD focusing on the time domain power difference in L-channel before and after the R-channel outputs. We optimized the matrix of the channel impulse response by using the downlink signal at 45° of elevation, 64APSK (4/5), and 29.3 dB of total XPD. We also trim a step-size parameter of the equalizer and the CFO estimation for various $E_s/(N_0 + I_{XPD})$. The thresholds of $E_s/(N_0 + I_{XPD})$ for 5,128,288 bits (= 100 frames) without bit error are 18.8 dB and 18.6 dB with R- and L-channel signals at 13° of elevation, respectively. The average $E_s/(N_0 + I_{XPD})$ of 18.7 dB indicates that the $E_s/(N_0 + I_{XPD})$ is 1.7 dB inferior to the threshold of signal in the laboratory room experiment as shown in Fig. 11. We consider that the 1.0 dB difference is associated with the insufficient compensation of the Doppler effects.

Figure 12 shows (a) E_s/N_0 versus angle of elevation

and (b) XPD, E_s/N_0 , and channel Signal to Interference plus Noise power Ratio (SINR) ($E_s/(N_0 + I_{XPD})$) versus angle of elevation, respectively. The satellite 3σ attitude error is about 1.2° , resulting in a 0.03 dB pointing loss for the 17 dBi gain antenna. At the ground station, we determine the satellite orbit parameter and the target angle for 10 m antenna pointing by using Two Line Element (TLE) provided by NORAD. The error is less than 0.1° (3.5 dB pointing loss). The 3 dB discrepancy between the calculation and the experiment in Fig. 12(a) is attributed to this pointing loss.

We evaluate the XPD with various angle of elevation based on the difference between E_s/N_0 and $E_s/(N_0 + I_{XPD})$. An XPD higher than that in Table 2 (Total XPD > 27 dB) is demonstrated when the angle of elevation $\geq 15^\circ$ as shown in Fig. 12(b).

Figure 13 presents 64APSK (4/5) constellation of (a) downlinked R- and (b) L-channel signals, respectively. The downlinked signal quality of R-channel is inferior to L-channel one because the nonlinear distortion in R-channel at a HPA is 1.3 dB larger than that in L-channel.

Table 8 shows the downlink experiment conditions, namely, Acquisition Of Signal (AOS), state of weather, modulation scheme, SINR, elevation and XPD. We evaluate noise tolerance with 64APSK (4/5) from 52.8 to 11.8° of elevation. Table 9 shows the stability of the communication after zenith showing various SINR. When $\text{SINR} \geq 22$ dB, BCH code is not used since the LDPC iteration does not reach the maximum number (= 50). Contrarily, when $\text{SINR} \leq 21$ dB, BCH code is used for compensation of Doppler effect, thermal noise and interference noise.

The demodulated binary data has no error compared with binary data obtained from the XTX in the laboratory room experiment. Consequently, we have achieved 2.65 Gbps in our satellite communication system with 300 Msps and polarization multiplexing of 64APSK (4/5) for RHCP and LHCP in the X-band. The frequency efficiency is $2.65 \text{ GHz}/315 \text{ MHz} = 8.41 \text{ bit/Hz}$.

7. Conclusions

In this paper, we have achieved 2.65 Gbps satellite downlink communication with 300 Msps and polarization multiplexing of 64APSK (4/5) for RHCP and LHCP in the X-band. The system has also realized a high frequency efficiency of 8.41 bit/Hz. We have developed the on-board XTX, the on-board dual circularly polarized-wave antenna, and the ground station system including the high XPD and high G/T antenna as well as the 300-Msps demodulator.

Acknowledgments

The authors would like to express the deepest appreciation to Yoshinori Kunii of Synspec Inc. for the fruitful discussion on the ground station antenna tracking algorithm, to Yasuhiko Miki and Yasuhiro Ohikata of Mebius Corporation and Masayuki Arai of Digital Signal Technology Inc. for the implementation of the XTX hardware and software.

References

- [1] H. Saito, P. Akbar, Rizki, V. Ravindra, T. Tomiki Atushi, H. Watanabe, J. Hirokawa, M. Zhang, o, and S. Shirasaka, "Compact X-band synthetic aperture radar with developable plane antenna and RF feed system through non-contact waveguides — Project of a 100 kg-class SAR satellite —," AIAA/Utah State University Small Satellite Conference, no. SSC17-IX-01, Utah, USA, Aug. 2018.
- [2] MathWorks, "Digitalglobe simulates complete satellite to ground communications systems," Feb. 2014.
- [3] A. Iwasaki and T. Tadano, "Future prospect on space communication infrastructure for remote sensing satellites," International Conference on Space Optical Systems and Applications (ICSOS), no.25, Kobe, Japan, May 2014.
- [4] K. Inaoka, M. Shirakura, M. Shimada, T. Sunaga, and N. Takata, "Development of an X-band multi-mode high-speed-modulator," *The Journal of Space Technology and Science*, vol.28, no.1, pp.12–21, 2013.
- [5] K. Devaraj, M. Ligon, E. Blossom, J. Breu, B. Klofas, K. Colton, and R. Kingsbury, "Planet high speed radio: Crossing Gbps from a 3U cubesat," AIAA/Utah State University Small Satellite Conference, no.SSC19VI01, Utah, USA, Aug. 2019.
- [6] K. Suzuki, M. Yahata, M. Kato, T. Watabe, K. Hoshi, T. Okui, S. Yoshikawa, M. Yoneda, Y. Arakawa, T. Asai, T. Takahashi, and M. Toyoshima, "16APSK/16QAM-OFDM 3.2 Gbps RF signal direct-processing transmitter and receiver communication experiments using WINDS satellite," Technical Committee on Space, Aeronautical and Navigational Electronics, IEICE, vol.115, no.241, pp.137–140, Oct. 2015.
- [7] K. Kaneko, H. Nishiyama, N. Kato, A. Miura, and M. Toyoshima, "Construction of a flexibility analysis model for flexible high-throughput satellite communication systems with a digital channelizer," *IEEE Trans. Veh. Technol.*, vol.67, no.3, pp.2097–2107, March 2018.
- [8] T. Kaneko, H. Saito, and A. Hirose, "SRAM: A septum-type polarizer design method based on superposed even- and odd-mode excitation analysis," submitted.
- [9] T. Kaneko, Y. Ohikata, M. Mita, and H. Saito, "2 Gbps downlink system of 100 kg class satellite for compact synthetic aperture radar mission," Small Satellite System and Services symposium, Sorrento, Italy, May-June 2018.
- [10] T. Kaneko, H. Saito, M. Mita, and Y. Ohikata, "Dual circularly polarization X band 2 Gbps downlink communication system of earth observation satellite," AIAA/Utah State University Small Satellite Conference, no.SSC18-XII-01, Utah, USA, Aug. 2018.
- [11] European Telecommunications Standards Institute (ETSI), Digital Video Broadcasting (DVB); Second generation framing structure, channel coding and modulation systems for Broadcasting, Interactive Services, News Gathering and other broadband satellite applications (DVB-S2), Aug. 2009.
- [12] European Telecommunications Standards Institute (ETSI), Digital Video Broadcasting (DVB); Second generation framing structure, channel coding and modulation systems for Broadcasting Interactive Services, News Gathering and other broadband satellite applications; Part 2: DVB-S2 Extensions (DVB-S2X), Oct. 2014.
- [13] S.-M. Kim, C.-S. Park, and S.-Y. Hwang, "A novel partially parallel architecture for high throughput-LDPC decoder for DVB-S2," *IEEE Trans. Consum. Electron.*, vol.56, no.2, pp.820–825, July 2010.
- [14] ITU. Rec. ITU-R SA.1157-1 "RECOMMENDATION ITU-R SA.1157-1" Protection criteria for deep-space research, 1995–2006.
- [15] European Telecommunications Standards Institute (ETSI), Digital Video Broadcasting (DVB); Implementation guidelines for the second generation system for Broadcasting, Interactive Services, News Gathering and other broadband satellite applications; Part 2: S2 Extensions (DVB-S2X), Nov. 2015.
- [16] H. Fukuchi, T. Kozu, Y. Takahashi, Y. Otsu, T. Oda, T. Mori,

- K. Nishimuta, and A. Suzuki, "Radio wave propagation experiments at the MTRS," *Quarterly Review of the Radio Research Laboratories*, vol.32, pp.37–56, Jan. 1986 (in Japanese).
- [17] ITU, Rec. ITU-R P.618-13, "Recommendation ITU-R P.618-1," Propagation Data and Prediction Methods Required for the Design of Earth-Space Telecommunication Systems, Dec. 2017.
- [18] ITU, Rec. ITU-R PN.837-1, "Recommendation ITU-R PN.837-1," Characteristics of Precipitation for Propagation Modelling (Question ITU-R 201/3), Dec. 2017.
- [19] ITU, Rec. ITU-R P.839-1, "Recommendation ITU-R P.839-1," Rain Height Model for Prediction Methods (Question ITU-R 201/3), 1992–1997.
- [20] ITU, Rec. ITU-R P.838-3, "Recommendation ITU-R P.838-3," Specific Attenuation Model for Rain for Use in Prediction Methods (Question ITU-R 201/3), 1992–1999–2003–2005.
- [21] E.R. De Lima, F.R.Q. Augusto, and J. Beetuzzo, "Design and FPGA prototyping of a DVB-S2 receiver: Towards a VLSI implementation in CMOS," 3rd Workshop on Circuits and System Design, Fortaleza, Brazil, Sept. 2013.
- [22] R. Peters, E. Klein-Lebbink, V. Lee, J. Model, R. Wezalis, and J. Taylor, "Applying EVM to satellite on-ground and in-orbit testing: Better data in less time," 26th International Communications Satellite System Conference (ICSSC), no. AIAA 2008-5508, June 2008.
- [23] Z. Wu, C. Zhang, F. Li, and W. Zhihua, "High speed serial interface transceiver controller based on JESD204B," 2016 14th IEEE International New Circuits and Systems Conference (NEWCAS), pp.26–29, Vancouver, Canada, June 2016.
- [24] C. Dudak and N.D. Kahyaoglu, "A descriptive study on AM-AM and AM-PM conversion phenomena through EVM-SNR relation," 2012 IEEE Topical Conference on Power Amplifiers for Wireless and Radio Applications, pp.15–18, Santa Clara, CA, USA, 2012.
- [25] T.R. Cunha, P.M. Cabral, and L.C. Nunes, "Characterizing power amplifier static AM/PM with spectrum analyzer measurements," 2014 IEEE 11th International Multi-Conference on Systems, Signals & Devices (SSD14), pp.11–14, Barcelona, Spain, May 2014.
- [26] T. Kaneko, S. Morisawa, and H. Saito, "Right and left circular polarized wave antenna for small satellite," Topical Workshop on Internet of Space (TWIOS), pp.13–16, Phoenix, AZ, USA, Jan. 2017.
- [27] T. Kaneko and H. Saito, "Dual circularly polarization antenna with high XPD for downlink communication of earth observation satellite," Conference on Antenna Measurements & Applications (CAMA) Tsukuba, pp.232–234, Tsukuba, Japan, Dec. 2017.
- [28] T. Kitsuregawa, *Advanced Technology in Satellite Communication Antennas: Electrical and Mechanical Design* (Artech House Antenna Library), House Antenna Library, Jan. 1990.
- [29] M.H. Chen and G.N. Tsandoulas, "A wide-band square waveguide array polarizer," *IEEE Trans. Antennas Propag.*, vol.AP-21, no.3, pp.389–391, May 1973.
- [30] M. Viswanathan, Ed., *Digital Modulations using MATLAB*, June 2017.
- [31] V. Saranya and M.T. BabiMol, "Adaptive feedback based normalized channel equalizer using minimal symbol-error-rate approach," *International Journal of Innovative Research in Science, Engineering and Technology*, pp.1662–1667, March 2014.



Tomoki Kaneko received the B.E. degree in Aerospace Engineering and the M.E. degree in Electronic Engineering from College of Science and Technology (CST), Nihon University, Tokyo, in 2015 and 2017 respectively. He has belonged to Ph.D. course at the Graduate School of Electrical Engineering in The University of Tokyo since 2017. His current research interests include wireless communication system for spacecraft, microwave waveguide, and neural network.



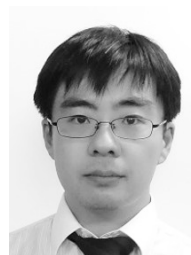
Noriyuki Kawano received the M.E. degree in Electronic Engineering and the Ph.D. in Informatics from Kyoto University. He is working at DLR and JAXA from 2008. His research interests include system design and signal processing for radar system, especially for Synthetic Aperture Radar (SAR).



Yuhei Nagao received the M.E and Ph.D. degrees in Graduate School of Computer Science from Kyushu Institute of Technology in 2006 and 2009, respectively. He had been a doctor researcher since 2009. He has joined Radrix Inc since 2012 and been visiting associate professor since 2016. He is engaged in chip developments of wireless LAN and its applications.



Keishi Murakami received B.E. and M.E. degrees in electronics and communication engineering from Waseda University, Tokyo, Japan, in 1974 and 1976, respectively. Since 1976, he has been engaged in research and development on digital satellite communication systems, digital mobile communication systems and various wireless communication systems, especially in the technical field of modulation/demodulation and wireless signal processing in Mitsubishi Electric Corporation. He joined research and development project of a small SAR satellite at JAXA in 2018. He is currently Senior Advisor of a startup company "Synspecrive" and developing a small SAR satellite system. He is a member of the IEEE.



Hiromi Watanabe received the M.S. degree in the Graduate School of Science from The University of Tokyo. He graduated Graduate School of Electrical Engineering in The University of Tokyo. He is a research assistant professor in School of System Design and Management, Keio University. He is engaged in radio frequency circuit, electronics technology, and satellite system technology.



Makoto Mita received the B.E. degree in Electronic Engineering from Tohoku University, Sendai, Japan, in 1996, and the M.E. and Ph.D. degrees in Electrical Engineering from The University of Tokyo, Tokyo, Japan, in 1999 and 2002, respectively. Since 2003, he has been an Assistant Professor with the Institute of Space and Astronautical Science, Japan Aerospace Exploration Agency, Sagami-hara, Japan. His research interests include microelectromechanical systems for space applications and nanomechanics.

tronics.



Takahisa Tomoda received the B.E. degree in Electronic Engineering from Chiba University in 1979. He had been engaged in development of electronics instruments for automobile from 1979 to 2013, and in a study of a small SAR satellite in JAXA since 2013 to 2019. He is currently a senior adviser of a startup company "Synspec-tive" and developing a small SAR satellite.



Keiichi Hirako received the B.S. and B.E. degrees in Mechanical Engineering from Osaka University. He is a project professor of Keio University in charge of senior adviser of a startup company "Synspec-tive" and developing a small SAR satellite. Since 1978 through 2014 he has been working for developments of old and new space satellites as a control engineer, system engineer, and a project manager at companies and JAXA.



Seiko Shirasaka received the M.E. degree in Astronautics from The University of Tokyo and Ph.D. in Systems Engineering from Keio University. He worked for Mitsubishi Electric Corporation as a space systems engineer for 15 years. He had been an Associate Professor at Keio University since 2008 and he has been a Professor since 2017. He was a program manager on Japanese government funded program ImPACT from 2015 through 2019.



Shinichi Nakasuka received the B.E., M.E., and Ph.D. degrees in Astronautics from The University of Tokyo in 1983, 1985, and 1988, respectively. He joined IBM Research during 1988–1990, and then worked for Department of Aeronautics and Astronautics, University of Tokyo as a lecturer in 1990, as an Associate Professor, and became a Professor in 2004. He is a member of JSASS, SICE, IAA, the former Chairperson of IFAC Aerospace Technical Committee, and current president of UNISEC-GLOBAL. His major

research areas include micro/nano/pico-satellites, autonomy and intelligence for space systems, novel space systems, and guidance, navigation and control of spacecraft. He developed and launched 9 micro/nano/pico-satellites successfully including the world first CubeSat.



Hirobumi Saito received the B.S., M.S., and Ph.D. degrees in Electrical Engineering from The University of Tokyo, Tokyo, Japan, in 1976, 1978, and 1981 respectively. He had been engaged in research of small satellite engineering at the Institute of Space and Astronautical Sciences, Japan Aerospace Exploration Agency, and he is currently the Emeritus Professor. He is also a visiting professor of Waseda University. He has authored or co-authored more than 50 scientific papers and 2 books. His current research

interests include the high-bit-rate downlink communications and the SAR system onboard small satellites. Dr. Saito is a member of the International Academy of Astronautics and IEICE. He was a recipient of the Technology Prize of Japan Society for Aeronautical and Space Sciences in 2010 and the Minister prize of Education, Science and Technology, Japan in 2012.



Akira Hirose received the Ph.D. degree in Electronic Engineering from The University of Tokyo in 1991. In 1987, he joined Research Center for Advanced Science and Technology (RCAST), the University of Tokyo, as Research Associate. In 1991, he was appointed as Instructor at RCAST. From 1993 to 1995, on leave of absence from The University of Tokyo, he joined the Institute for Neuroinformatics, University of Bonn, Bonn, Germany. He is currently Professor with the Department of Electrical Engineering

and Information Systems, The University of Tokyo. The main fields of his research interests are wireless electronics and neural networks. In the fields, he published several books such as Complex-Valued Neural Networks, 2nd Edition (Springer 2012). He served as the General Chair of several international conferences such as International Geoscience and Remote Sensing Symposium (IGARSS) 2019 Yokohama. Dr. Hirose is a Fellow of the IEEE and the IEICE, and a Member of JNNS and APNNS.